Baroclinic and Barotropic Instabilities of Coastal Currents

L. A. MYSAK,[1] E. R. JOHNSON[2] AND W. W. HSIEH

Department of Oceanography, University of British Columbia, Vancouver, B.C., Canada V6T 1W5

(Manuscript received 15 August 1979, in final form 17 September 1980)

ABSTRACT

The two-layer baroclinic instability model of the California Undercurrent from Mysak (1977) is modified to investigate the effects of the lateral boundary conditions on the stability properties of the system. As is common in baroclinic instability calculations, Mysak (1977) assumes the mean flow along the continental rise to be bounded laterally by vertical rigid walls, thus allowing the cross-stream structure of the perturbation flow to be decomposed into simple normal modes. Instability then occurs when waves of the same cross-stream structure interact. The dominant instability is that associated with the gravest mode.

In the first model presented here we consider the effect of replacing the rigid outer boundary with a quiescent, constant-depth ocean. Waves of short longshore wavelength are not greatly affected by the open seaward boundary. However, as consideration is turned to waves of longer longshore wavelength, the cross-stream wavenumber departs further from the integral values of the channel-flow problem and another class of baroclinic instabilities occurs due to interaction between waves of differing cross-stream structure. Nevertheless, the dominant baroclinic instability remains that associated with the gravest mode. A new barotropic instability is also present, drawing energy from the horizontal shear between the coastal current and the quiescent ocean.

In the second model the rigid outer boundary is retained but the inner boundary is replaced by a shallow sloping region, modeling the effects of a sloping shelf adjoining the coastal current which flows along the continental rise. Topographic waves are present above the sloping inshore region. These waves are coupled with the channel waves. Once again the cross-stream wavenumber departs from the integral values of the channel problem and instabilities are present due to interaction between waves of differing cross-stream structure. As in the previous model the dominant baroclinic instability is that of the gravest mode and a new barotropic instability is present due to the lateral shear in the mean flow at the shelf break.

For both models, a parameter study is presented in which we determine the effects of varying the shear, stratification and bottom slope.

1. Introduction

In a number of recent studies, a quasi-geostrophic two-layer baroclinic instability model with vertical rigid side walls and a sloping bottom has been used to help explain the mesoscale fluctuations observed in various coastal flows (Smith, 1976; Mysak, 1977; Mysak and Schott, 1977; Helbig, 1978; Emery and Mysak, 1980). Generally speaking, the length and time scales of the observed fluctuations compare quite favorably with the wavelength and period of the most unstable waves. However, despite this qualitative agreement between theory and observation, it is natural to ask whether the unstable baroclinic waves in a channel model are significantly affected if the vertical side walls are replaced by other boundaries, representing either the open ocean or the continental shelf. The main purpose of this paper is to investigate analytically, via two simple models, the effects of different lateral boundary conditions on the stability properties of a two-layer geostrophic flow along a sloping bottom which represents the continental rise. In previous theoretical studies which have investigated this baroclinic instability problem, the associated eigenvalue problem has been solved numerically and the results are generally quite complex (e.g., see Orlanski and Cox, 1973; Hart, 1974; Cutchin and Rao, 1976; Kubota, 1977; Wright, 1980).

By adding a quiescent open ocean or continental shelf to the simple channel-flow model, the possibility of barotropic instability now exists because of the horizontal shear in the mean flow. A second purpose of this paper, therefore, is to introduce into the literature two simple analytical models for the combined baroclinic-barotropic instability problem for coastal flows. The combined baroclinic-barotropic instability problem has received considerable attention during the last decade. However, generally speaking the studies of this problem have either treated laterally unbounded flows with weak horizontal shear (Stone, 1969; McIntyre, 1970; Gent, 1975;

[1] Also Department of Mathematics, University of British Columbia.

[2] Present affiliation: Department of Mathematics, University College London, London, England.

0022-3670/81/020209-22$09.50

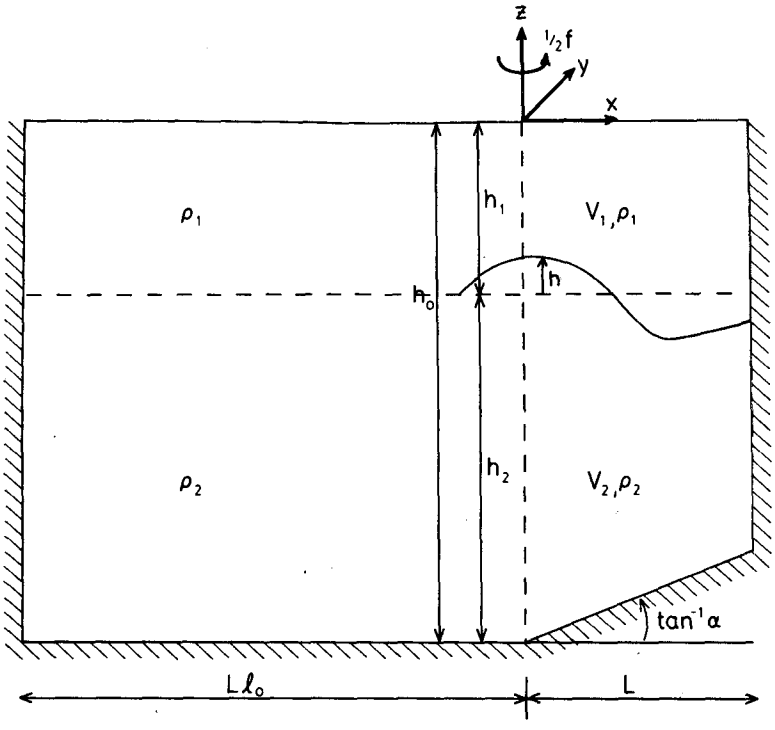

FIG. 1. Flow system considered in open-ocean model. The nondimensional instantaneous interfacial height due to the mean flow and the traveling wave disturbance is given by $h = (V_2 - V_1)x + \phi_2 - \phi_1$, where V_n, x and ϕ_n are the nondimensional quantities used in Section 2. In terms of dimensional V_n, x and ϕ_n (the latter having dimensions of streamfunction), the dimensional instantaneous interfacial height is given by $(f/g')[(V_2 - V_1)x + \phi_2 - \phi_1]$.

Killworth, 1980) or coastal flows with complex lateral structures that require extensive numerical computations (see references cited at the end of first paragraph).

In Section 2 we consider, for the California Undercurrent parameters used by Mysak (1977), the effect of replacing the rigid outer boundary of the flow with a quiescent, constant-depth ocean. While short waves are not greatly affected by the open boundary, the long waves have associated cross-stream wavenumbers that differ considerably from the integral values of the channel-flow problem and another class of baroclinic instabilities occurs due to interactions of waves of differing cross-stream structure. A barotropic instability also is present in this model due to the horizontal shear between the coastal current and the quiescent ocean. In Section 3 we investigate the effects of varying the shear, stratification and topographic parameters in the open ocean model. In Section 4 the rigid outer boundary is retained but the inner boundary is replaced by a shallow sloping region, modeling the effects of a sloping shelf adjoining the coastal current. In both this section and Section 2, we use the same shear, stratification and topographic parameters for the continental rise region as in Mysak (1977). Quasi-geostrophic topographic waves[3] are present above the sloping inshore region, and these waves are coupled with the channel waves. Once again the cross-stream wavenumber departs from the integral values of the channel problem and instabilities are present due to the interaction between waves of differing cross-stream structure. There also is present a barotropic instability due to the shear between the coastal current and a longshore shelf current. In Section 5 we investigate the effects of varying the parameters characterizing the shears, stratification and topography in the shelf model.

2. Open ocean model

We consider a two-layer geostrophic flow in a uniformly rotating channel above a lower boundary which consists of a sloping region and a constant depth outer region (Fig. 1). The variables are nondimensionalised using L and h_0 for the horizontal

[3] These waves are not to be confused with the familiar continental shelf waves (for a review see Mysak, 1980), which are aegeostrophic in the longshore direction since their wavelength is much larger than the shelf width (Pedlosky, 1979, Section 8.2).

and vertical scales, L/U for the time scale, U and h_0U/L for the horizontal and vertical velocity scales, and $\rho_n fUL$ for the non-hydrostatic pressure scale in layer n ($n = 1, 2$). For flow at small Rossby number, ($U/fL \ll 1$), Pedlosky (1964) shows that small perturbations to the flow satisfy

$$\left.\begin{aligned}&(\partial_t + U_1\partial_y)[\Delta\phi_1 + F_1(\phi_2 - \phi_1)]\\&\quad + [F_1(U_1 - U_2) - U_{1xx}]\phi_{1y} = 0\\&(\partial_t + U_2\partial_y)[\Delta\phi_2 + F_2(\phi_1 - \phi_2)]\\&\quad - [F_2(U_1 - U_2) + T + U_{2xx}]\phi_{2y} = 0\end{aligned}\right\}, \quad (2.1)$$

where $\Delta = \partial_{xx} + \partial_{yy}$, $U_n(x)$ is the basic geostrophic velocity along the channel and ϕ_n the perturbation streamfunction in layer n, which has been scaled by UL. The nondimensional parameters are

$$F_1 = f^2L^2/g'h_1, \quad F_2 = f^2L^2/g'h_2, \quad T = \alpha fL^2/Uh_2,$$

where $g' = g(1 - \rho_1/\rho_2)$ is the reduced gravity and α is the bottom slope. The boundary condition of no normal flow at the side boundaries gives

$$\phi_{ny} = 0, \quad n = 1, 2, \quad \text{at} \quad x = 1, -l_0.$$

We look for solutions of the form

$$\phi_n = \mathrm{RE}\{\exp[ik(y - ct)]\psi_n(x)\},$$

such that the ψ_n satisfy

$$(c - U_1)[\psi_{1xx} - k^2\psi_1 + F_1(\psi_2 - \psi_1)] - [F_1(U_1 - U_2) - U_{1xx}]\psi_1 = 0, \quad (2.2a)$$

$$(c - U_2)[\psi_{2xx} - k^2\psi_2 + F_2(\psi_1 - \psi_2)] + [F_2(U_1 - U_2) + T + U_{2xx}]\psi_2 = 0, \quad (2.2b)$$

$$\psi_n = 0 \quad \text{at} \quad x = 1, -l_0. \quad (2.3)$$

We shall consider the case where the current flows solely above the sloping region and the adjoining ocean is quiescent, i.e.,

$$U_n(x) = \begin{cases} V_n, & n = 1, 2, \quad \text{if} \quad 0 < x \leq 1 \\ 0, & \text{if} \quad -l_0 \leq x < 0, \end{cases}$$

where V_n is a constant. We thus obtain solutions of (2.2) by solving the constant coefficient equations in the regions $0 < x \leq 1$ and $-l_0 \leq x < 0$ and then matching the solutions across $x = 0$. The first matching condition is obtained by integrating (2.2) from $-\epsilon$ to ϵ for $0 < \epsilon \ll 1$ and then taking the limit $\epsilon \to 0$. We find that $(c - U_n)\psi_{nx} + U_{nx}\psi_n$ must be continuous at $x = 0$. By integrating from $-\epsilon$ to x, dividing by $(c - U_n)^2$ and integrating from $-\delta$ to δ, we obtain this second condition that $\psi_n/(U_n - c)$ is continuous at $x = 0$.

The solution of (2.2) in $-l_0 \leq x < 0$ subject to (2.3) is

$$\left.\begin{aligned}\psi_1 &= a_1 \sinh k(x + l_0) + a_2F_1 \sinh\kappa(x + l_0)\\ \psi_2 &= a_1 \sinh k(x + l_0) - a_2F_2 \sinh\kappa(x + l_0)\end{aligned}\right\}, \quad (2.4)$$

where $\kappa^2 = k^2 + F_1 + F_2$, and a_1 and a_2 are arbitrary constants. The general solution of (2.2) in $0 < x \leq 1$ subject to (2.3) is

$$\left.\begin{aligned}\psi_2 &= a_3F_1 \sinh r_1(x - 1) + a_4F_1 \sinh r_2(x - 1)\\ \psi_2 &= a_3R_1 \sinh r_1(x - 1) + a_4R_2 \sinh r_2(x - 1)\end{aligned}\right\}, \quad (2.5)$$

where

$$R_1 = \tfrac{1}{2}[S + (S^2 + 4F_1F_2)^{1/2}],$$

$$R_2 = \tfrac{1}{2}[S - (S^2 + 4F_1F_2)^{1/2}],$$

$$S = F_1(V_2 - c)/(V_1 - c) - [F_2(V_1 - c) + T]/(V_2 - c),$$

$$r_n^2 = R_n - k^2 - F_1(V_2 - c)/(V_1 - c), \quad n = 1, 2,$$

and a_3 and a_4 are arbitrary constants. Applying the matching conditions[4] gives a system of four equations, linear in the four unknowns a_1, a_2, a_3, a_4, i.e.,

$$\mathbf{Aa} = \mathbf{0}, \quad (2.6)$$

where $\mathbf{a} = (a_1, a_2, a_3, a_4)^{\mathrm{T}}$, and

$$\mathbf{A} = \begin{pmatrix} (c - V_1)F_1 \tanh\kappa l_0 & (c - V_1)\tanh kl_0 & cF_1 \sin r_1 & cF_1 \sin r_2 \\ cF_1\kappa & ck & (V_1 - c)F_1r_1 \cos r_1 & (V_1 - c)F_1r_2 \cos r_2 \\ (V_2 - c)F_2 \tanh\kappa l_0 & (c - V_2)\tanh kl_0 & cR_1 \sin r_1 & cR_2 \sin r_2 \\ -cF_2\kappa & ck & (V_2 - c)R_1r_1 \cos r_1 & (V_2 - c)R_2r_2 \cos r_2 \end{pmatrix}. \quad (2.7)$$

System (2.6) will have nontrivial solutions for $\mathbf{a}$ if and only if the determinant of $\mathbf{A}$ vanishes. Thus the dispersion relation is

$$\det\mathbf{A} = 0. \quad (2.8)$$

In the limit $l_0 \to 0$, (2.8) reduces to the dispersion relation given by Mysak (1977), with solutions $r_1 = m\pi$ or $r_2 = m\pi$, $m = \pm1, \pm2, \pm3, \ldots$. A plot of the dispersion curves for $V_1 = 1$, $V_2 = 0.25$, $l_0 = 0$,

[4] Note that for the mean flow under consideration, the first matching condition reduces to $(c - U_n)\psi_{nx}$ continuous at $x = 0$.

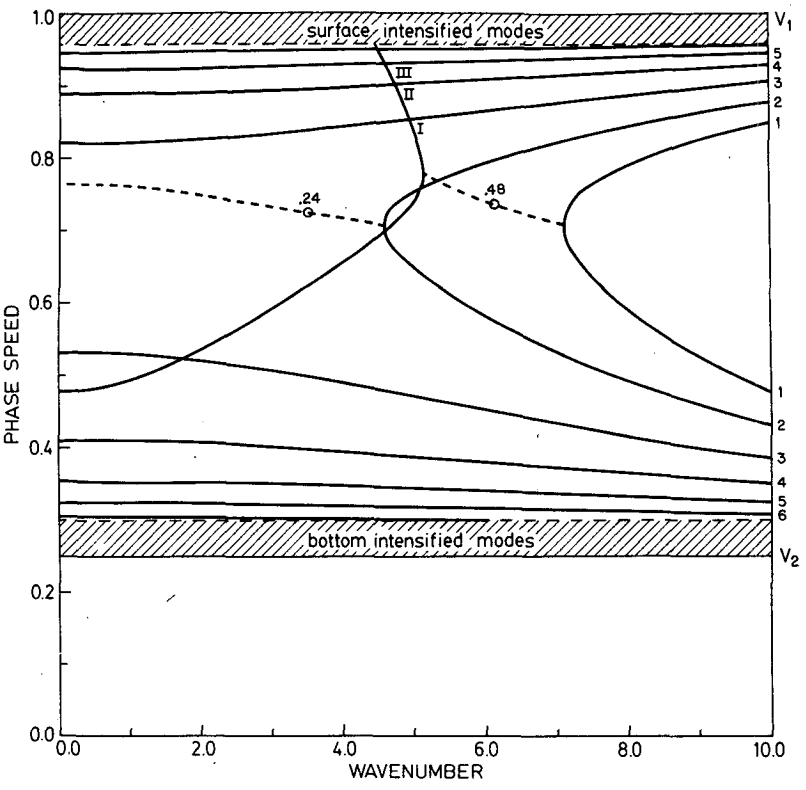

FIG. 2. Dispersion curves Re(c) vs k for channel flow. $V_1 = 1$, $V_2 = 0.25$, $F_1 = 27$, $F_2 = 6.8$, $T = 21$, $l_0 = 0$, which are representative of the California Undercurrent off Vancouver Island (Mysak, 1977). The solid lines represent stable waves and the dashed lines give the real part of the phase speed for the unstable wave. For each instability the position of the maximally unstable wave is marked by a circle and its nondimensional growth rate noted. The dispersion curves are labeled by cross-stream mode numbers.

$F_1 = 27, F_2 = 6.8$ and $T = 21$[5] [values used in Mysak (1977) for the California Undercurrent] is given in Fig. 2. The shaded regions below $c = V_1$ and above $c = V_2$ correspond to regions where there are an infinite number of discrete higher modes. There is baroclinic instability whenever the upper and lower wave of same cross-stream mode have the same phase speed. For the parameter values in Fig. 2 this occurs only for cross-stream modes one and two. No other interactions occur. Where two curves cut, (e.g., I, II, III) two different cross-stream modes exist with the same phase speeds but do not interact. The circles in Fig. 2 show the location of the fastest growing unstable waves. The nondimensional growth rates Im(kc) are also given at these points. The growth rate of the gravest mode is twice that of the second mode and so the dominant instability is the fundamental mode instability.

Fig. 3 shows the same situation for $l_0 \to \infty$. This value is chosen as the most extreme. However, Fig. 3 is typical of dispersion curves for $l_0 > 1$. For large k (i.e., short wavelengths), the waves are unaffected by the absence of a rigid outer boundary at $x = 0$. The maximally unstable baroclinic wave remains that associated with the first mode and the growth rate, wavelength, etc., of this wave are within 2% of the channel case. However, for smaller k, that is for waves whose longshore wavelength is comparable or slightly longer than the width of the continental rise, the dispersion curves are modified significantly. Previously, the curve for the first mode cut those for the other modes without interacting. The corresponding points in Fig. 3 (i.e., I, II, III) show that instability is now present for these waves with similar phase speed but differing cross-stream structure. The instability I corresponds to an upper layer concentrated baroclinic mode one interacting with an upper layer mode three. The points IV, V and VI correspond to interactions between mode two and higher baroclinic modes. The largest growth rate for these baroclinic instabilities between waves of

[5] For values of T of this order, the inclusion of β would change the results by only ~1% and thus has been neglected in this study.

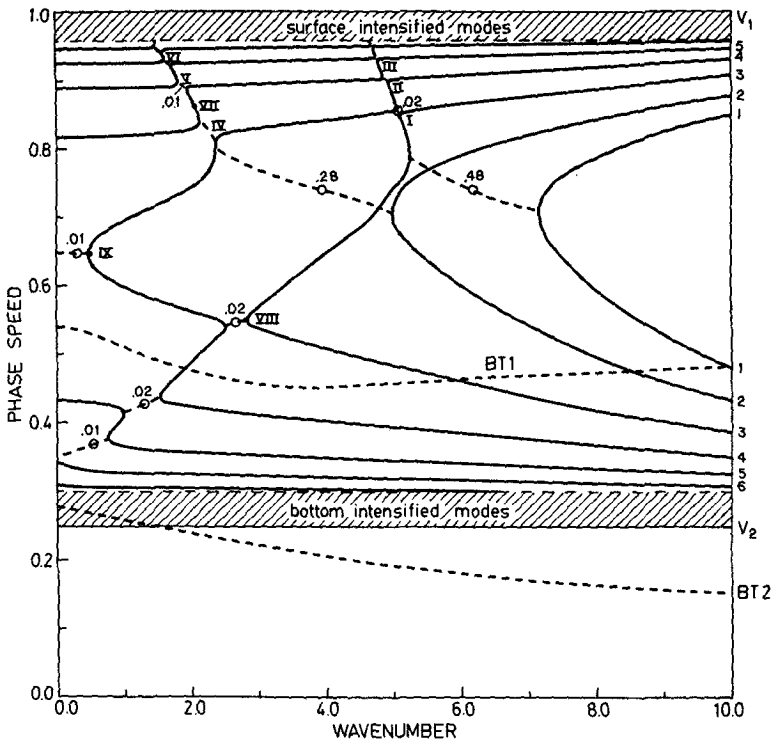

FIG. 3. Dispersion curves for the open-ocean model. The parameters are the same as in Fig. 2 with, however, l_0 infinite.

differing cross-stream structure is 0.02 for the one-three interaction (i.e., I), only 4% of that of the maximally unstable wave. On a given solid curve k is a single-valued function of c. Unstable waves first appear at the points on the dispersion curves where $\partial k/\partial c = 0$.

Figs. 4, 5 and 6 show the streamfunctions (to within a real multiplicative constant) for the stable waves

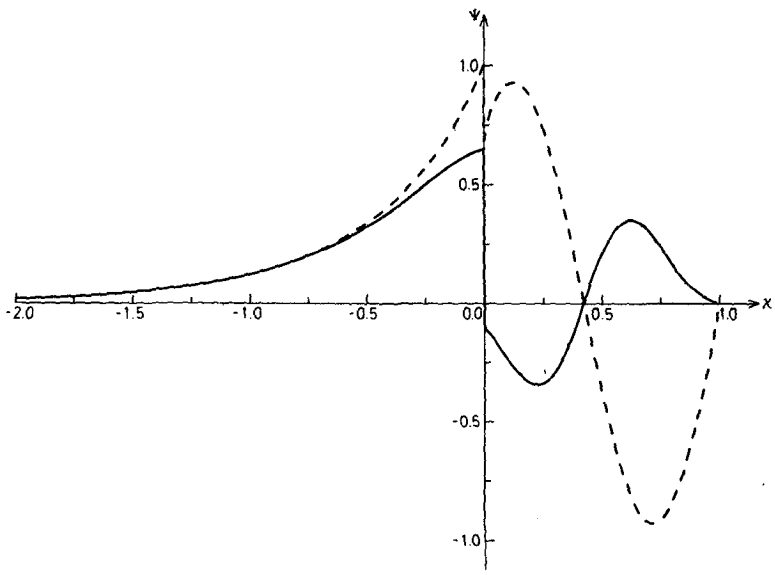

FIG. 4. Streamfunctions for the wave VII ($k = 2.05, c = 0.86$) of the ocean model. The solid line is the upper layer response, the dashed line that of the lower layer.

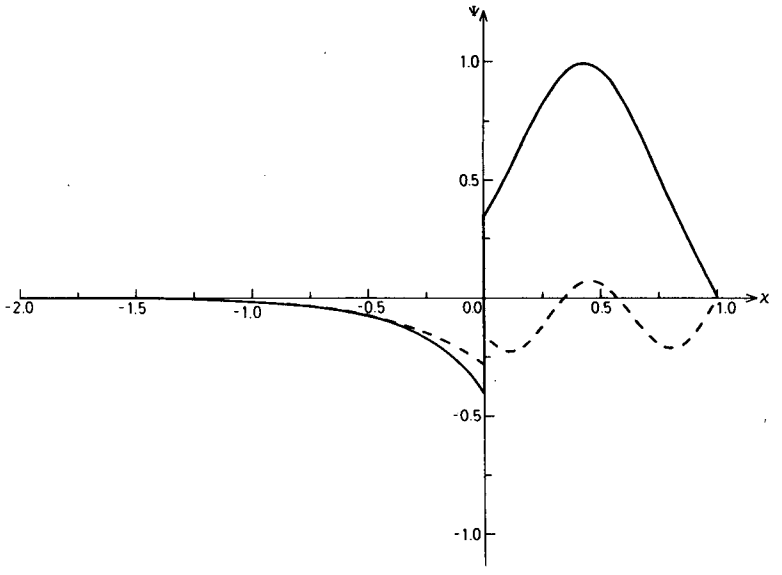

FIG. 5. Streamfunctions for the wave VIII ($k = 2.8, c = 0.55$) of the ocean model.

numbered VII ($k = 2.05, c = 0.86$), VIII ($k = 2.8$, $c = 0.55$) and IX ($k = 0.48$, $c = 0.65$) in Fig. 3. Wave VII (Fig. 4) lies away from a point of interaction of two waves and thus displays the characteristics of a stable wave in the channel model. The streamfunctions have very similar cross-stream structures for both the upper and lower layers (although out of phase by π) and the disturbance is a modified second mode (mode number ~ 1.7). In the quiescent ocean the disturbance decays monotonically. Wave VIII (Fig. 5) lies at the intersection of the dispersion curves for modes one and three. The wave contrasts with wave VII in showing a completely different modal structure in both layers. The lower layer is a modified third mode and the upper layer is a modified first mode. Such different vertical modal structure is not possible in the simple channel model.

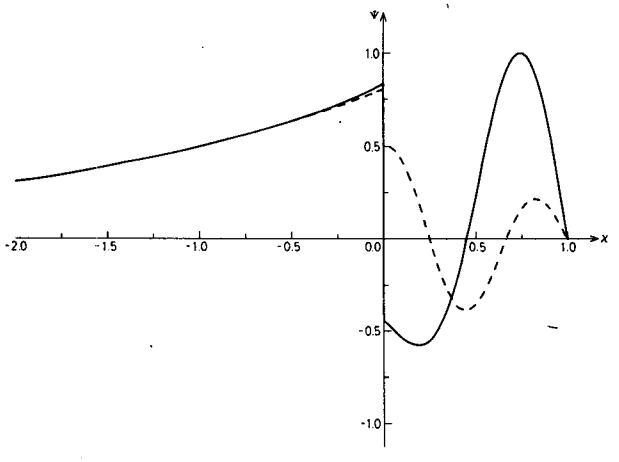

FIG. 6. Streamfunctions for the wave IX ($k = 0.48, c = 0.65$) of the ocean model.

For very long waves ($k \to 0$), the outer boundary of the current is an antinode for the waves and the wavenumbers approach ½, 3/2, 5/2, ... Wave IX (Fig. 6) consists of a bottom layer concentrated wave with mode number 2.5 interacting with an upper layer mode 1.6. Such long waves decay slowly in the open ocean.

Horizontal shear between the inner and outer fluid regions allows the flow to be barotropically unstable. The first two lines in Table 1 give the nondimensional growth rates for the waves (BT1 and BT2 in Fig. 3) caused by this shear. The waves are unstable at all wavelengths. At short wavelengths, the magnitudes of the real and imaginary parts of the phase speed approach half the velocity difference in the layer in which the wave is concentrated, i.e.,

$$c \to \tfrac{1}{2}V_n(1 \pm i) \quad \text{as} \quad k \to \infty \quad (n = 1, 2).$$

Thus an arbitrarily large growth rate can be obtained by choosing a sufficiently short wave which, however, will then be confined to a small region about $x = 0$. This effect is due to the unrealistic concentration of the velocity shear at $x = 0$.

With no vertical shear, and in the absence of topographic effects ($V_1 = V_2 = V$, $T = 0$), $r_1 = ik$ and $r_2 = i\kappa$, giving modes decaying exponentially from $x = 0$, with dispersion relation

$$[c^2 \tanh\kappa + (V - c)^2 \tanh\kappa l_0] \times [c^2 \tanh k + (V - c)^2 \tanh k l_0] = 0. \quad (2.9)$$

TABLE 1. Nondimensional growth rates Im(kc) of the barotropically unstable waves in the open-ocean model.

	V_1, V_2	F_1, F_2	T		Wavenumber k 1	2	4	6	8	10
FIG. 3	1, 0.25	27, 6.8	21	BT1	0.32	0.73	1.70	2.72	3.75	4.78
				BT2	0.10	0.23	0.55	0.87	1.15	1.41
FIG. 7	1, 0.0			BT1	0.31	0.66	1.54	2.58	3.64	4.69
				BT2	—	—	—	—	—	—
FIG. 8	1, −0.25			BT1	0.30	0.60	1.34	2.40	3.51	4.60
				BT2	0.04	0.11	0.23	0.37	0.52	0.70
FIG. 9	0.5, 0.0			BT1	0.15	0.31	0.76	1.29	1.82	2.35
				BT2	—	—	—	—	—	—
FIG. 10	1, 0.25	13.5, 3.4	21	BT1	0.32	0.77	1.79	2.83	3.86	4.88
				BT2	0.08	0.22	0.55	0.87	1.15	1.41
FIG. 11		54, 13.6		BT1	0.33	0.72	1.59	2.56	3.58	4.61
				BT2	0.10	0.24	0.55	0.87	1.16	1.42
FIG. 12	1, 0.25	27, 6.8	42	BT1	0.31	0.70	1.68	2.71	3.75	4.78
				BT2	0.07	0.19	0.50	0.84	1.16	1.45
FIG. 13			10.5	BT1	0.34	0.75	1.69	2.71	3.74	4.78
				BT2	0.11	0.26	0.58	0.86	1.13	1.37
FIG. 14			0.0	BT1	0.28	0.56	1.64	2.69	3.74	4.78
				BT2	0.14	0.30	0.57	0.82	1.06	1.30

These waves are the two-layer equivalent of those given by Drazin and Howard (1966) for barotropic instability in channel flow. The roots of (2.9) are two complex conjugate pairs and so the waves are unstable at all wavelengths.

3. Parameter study of open ocean model

In Section 2 and in Figs. 2–6, the values for V_n, F_n and T are representative of the California Undercurrent off Vancouver Island (Mysak, 1977). In this section we shall illustrate how the dispersion curves and growth rates are affected by varying the above parameters, which characterize the shear, stratification and topography of the mean state, respectively.

Figs. 7–9 show the dispersion curves for new values of V_n and should be compared with Fig. 3, where $(V_1, V_2) = (1, 0.25)$. As might be anticipated, by increasing the vertical shear $V_1 - V_2$ (Figs. 7 and 8), the wavenumber range of baroclinic instability for the first two cross-channel modes is increased substantially, with a shift toward lower wavenumbers. Also, the maximal growth rates have nearly doubled (Fig. 8). There is also a corresponding increase in the growth rates of the secondary baroclinic instabilities. Thus, in general, larger vertical shears enhances the baroclinic instabilities, increasing their growth rates. For these larger vertical shears, the growth rates for the barotropically unstable waves are reduced—substantially for the BT2 wave, but only slightly for the BT1 wave. In particular, while the magnitudes of the horizontal shears in Fig. 8 are the same as those in Fig. 3, the increased vertical shear in Fig. 8 results in a BT2 wave growth rate that is only half as large (see Table 1). Fig. 9 shows the dispersion curves for a weaker vertical shear ($V_1 - V_2 = 0.5$) and also reduced lateral shears in the two layers. In this case the growth rates of the maximally unstable baroclinic waves (first two modes) have dropped by about a third, whereas the growth rates of the BT1 wave have dropped by more than a factor of 2 (see Table 1).

Figs. 10 and 11 show the dispersion curves for new values of F_n, with the other parameters unchanged. Halving F_1 and F_2 (Fig. 10) is equivalent to doubling $\Delta\rho/\rho$, i.e., increasing the stratification by a factor of two [see sentence following Eq. (2.1)]. Comparing Fig. 10 with Fig. 3, we note that while the baroclinic instabilities associated with modes 1 and 2 now have much smaller growth rates and wavenumber ranges, the secondary baroclinic instabilities have larger growth rates and wavenumber ranges. Thus stratification stabilizes the usual channel-mode baroclinic instabilities, but slightly destabilizes the secondary "interaction" instabilities! For weaker stratification (Fig. 11), on the other hand, the channel modes are considerably destabilized and the secondary modes slightly stabilized. For the barotropi-

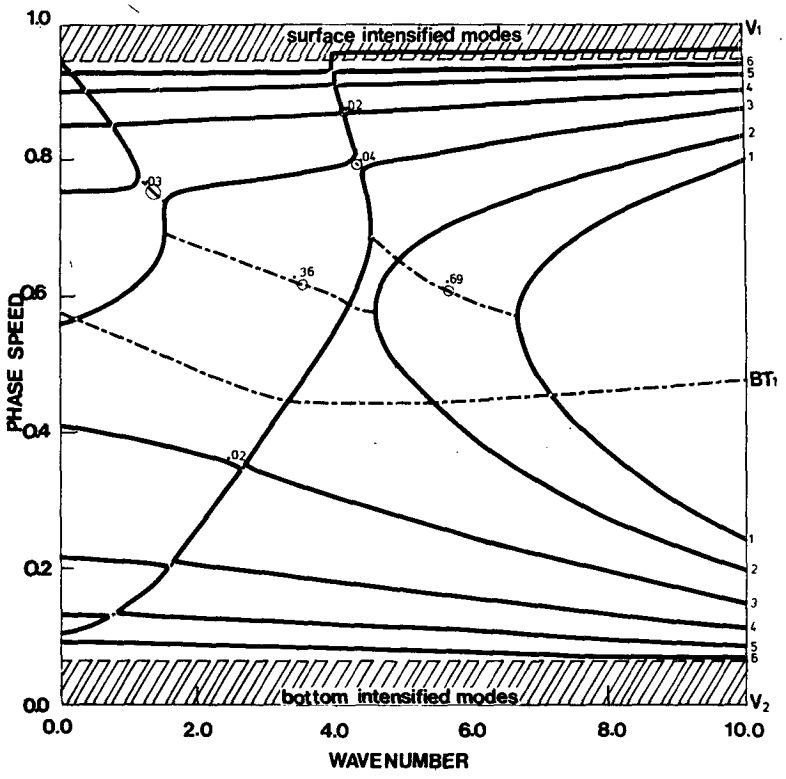

FIG. 7. As in Fig. 3 with $V_1 = 1$, $V_2 = 0.0$ (larger vertical shear).

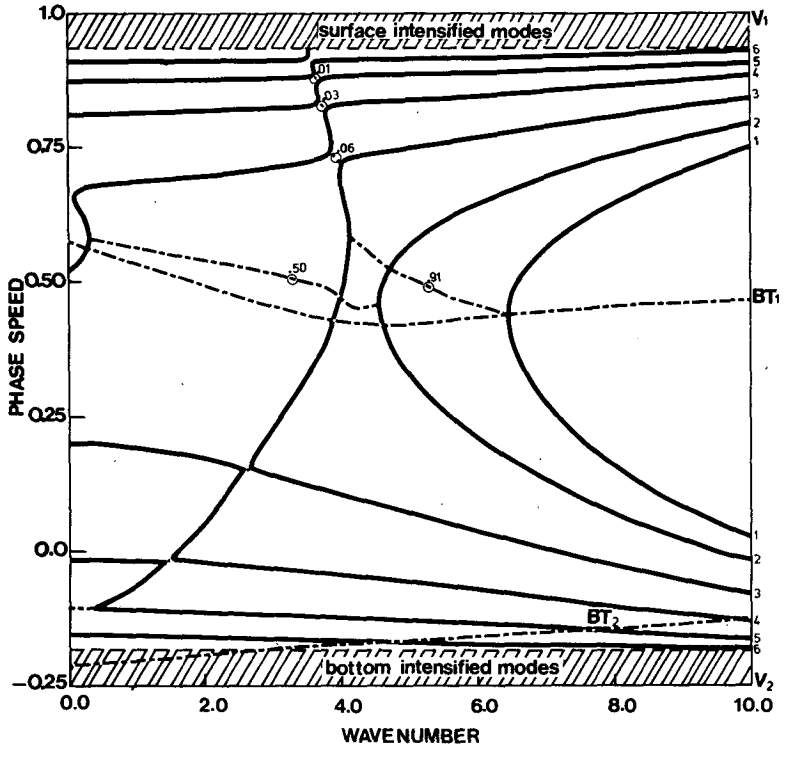

FIG. 8. As in Fig. 3 with $V_1 = 1$, $V_2 = -0.25$ (larger vertical shear).

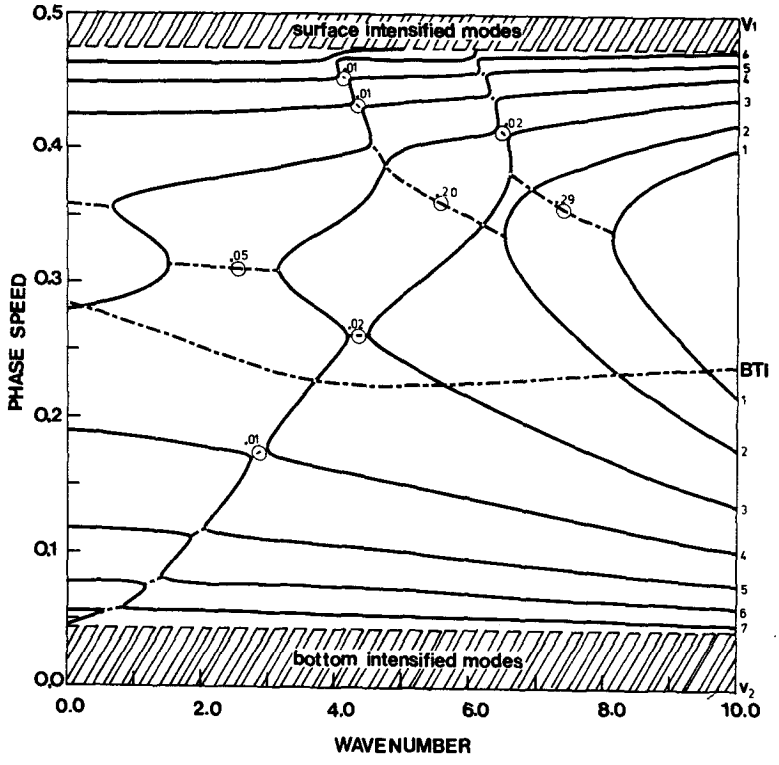

FIG. 9. As in Fig. 3 with $V_1 = 0.5, V_2 = 0.0$ (smaller vertical and horizontal shears).

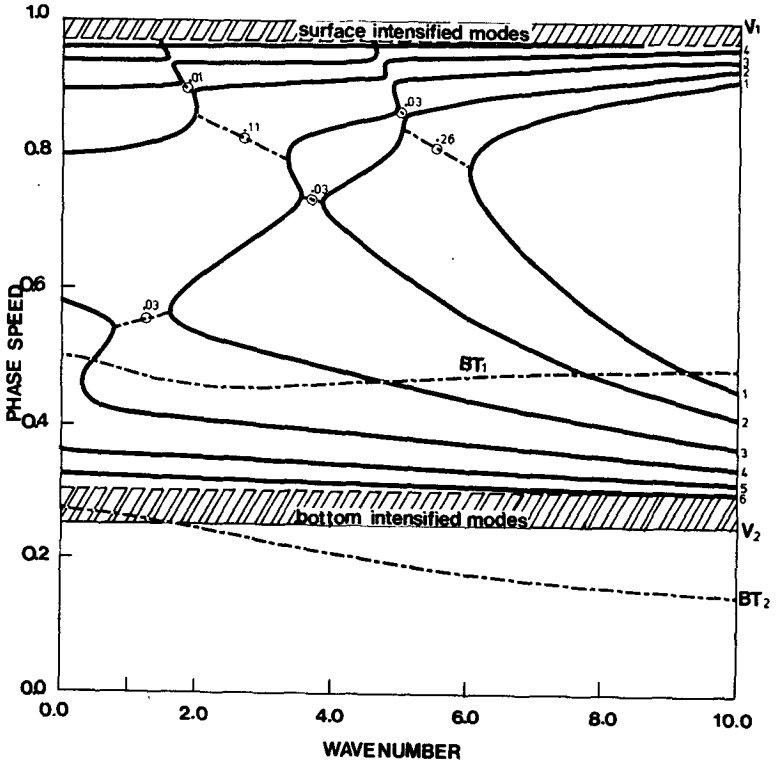

FIG. 10. As in Fig. 3 with $F_1 = 13.5, F_2 = 3.4$ (stronger stratification).

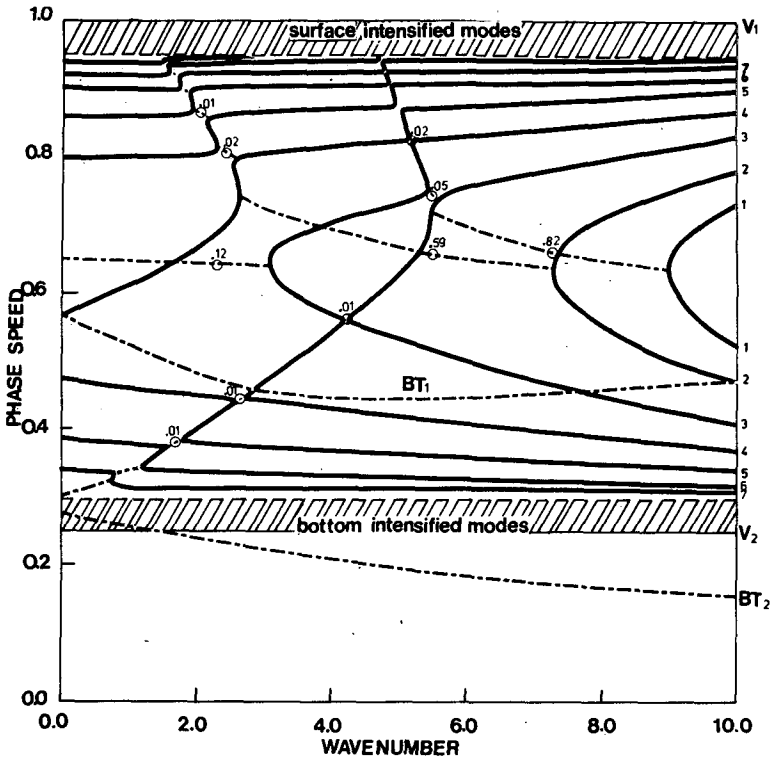

FIG. 11. As in Fig. 3 with $F_1 = 54$, $F_2 = 13.6$ (weaker stratification).

cally unstable waves, varying F_n has very little effect on the BT2 wave growth rates, but the BT1 wave growth rates increase (decrease) by 5–10% when $\Delta\rho/\rho$ is doubled (halved) (see Table 1).

Figs. 12–14 show that topography is both a stabilizing *and* complicating influence on the baroclinically unstable waves. For a larger bottom slope (Fig. 12, with $T = 42$), the wavenumber ranges for first and second mode instabilities have decreased and shifted to higher phase speeds and wavenumbers. However, only the maximum growth rate of the gravest mode has been substantially reduced. At lower wavenumbers, there are now new weak instabilities, both primary (involving higher cross-channel modes) and secondary. As the bottom slope tends to zero (Figs. 13 and 14), the dispersion curves simplify considerably, with the limiting case $T = 0$ (Fig. 14) representing the classical Eady model with an open ocean on one side. For this case the first cross-channel mode (only) is unstable for all $k \leq 4.3$ and its maximum growth rate (at $k = 2.1$) is comparable to the growth rate of the BT1 wave at that wavenumber. However, it is interesting to note the interaction between these two unstable waves near $k = 2.2$: as k decreases the dispersion curves slowly start to coalesce, but suddenly, at $k = 2.2$, rapidly diverge.

Varying T has little effect on the growth rates of the upper BT1 wave (as might be anticipated); however the growth rate of the lower BT2 wave can be significantly altered, especially at lower wavenumbers. As $T \to 0$, the growth rate of a long BT2 wave is nearly doubled (see Table 1).

4. Shelf model

We consider the effect of a shelf of width Ll_s adjoining a deep region of width L. In the light of the results in Section 2, we shall assume that the current in the deep region is bounded by a solid outer wall (Fig. 15). The inclusion of a quiescent unbounded outer ocean is straightforward but is omitted here to isolate the effect of the shelf and because of the small effect of the quiescent ocean on the maximally unstable baroclinic waves. We shall further simplify the problem by assuming that in the absence of any mean flow, the upper layer of the channel region is of the same thickness as the outer depth of the shelf. [Such a model has been considered by Gill and Clarke (1974) to study the importance of coastal trapped waves in upwelling.] However, when the mean and perturbation flow is included the position of the interface at $x = 1$ lies just below the shelf break, provided $V_2 - V_1 < 0$ and the perturbations ϕ_n are small (see Fig. 15). With this restriction on $V_2 - V_1$, the frontal problem in which the interface lies over the shelf, is avoided. The Eqs. (2.2)

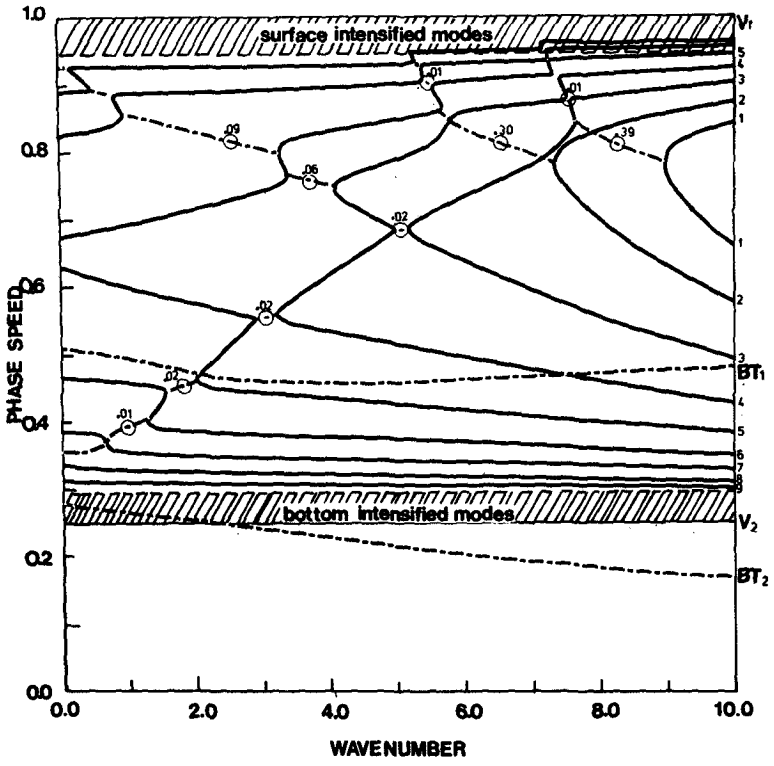

FIG. 12. As in Fig. 3 with $T = 42$ (larger bottom slope).

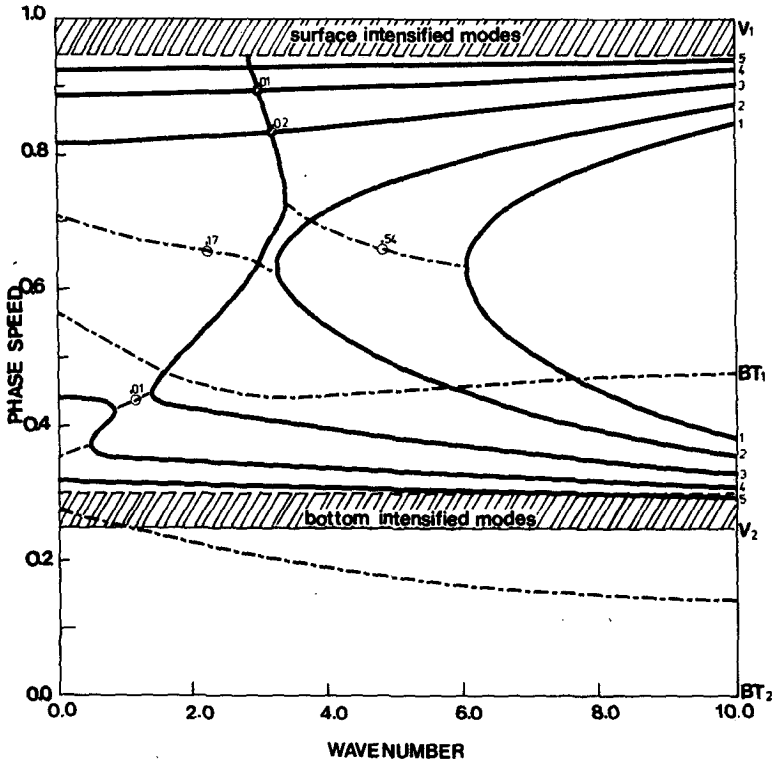

FIG. 13. As in Fig. 3 with $T = 10.5$ (smaller bottom slope).

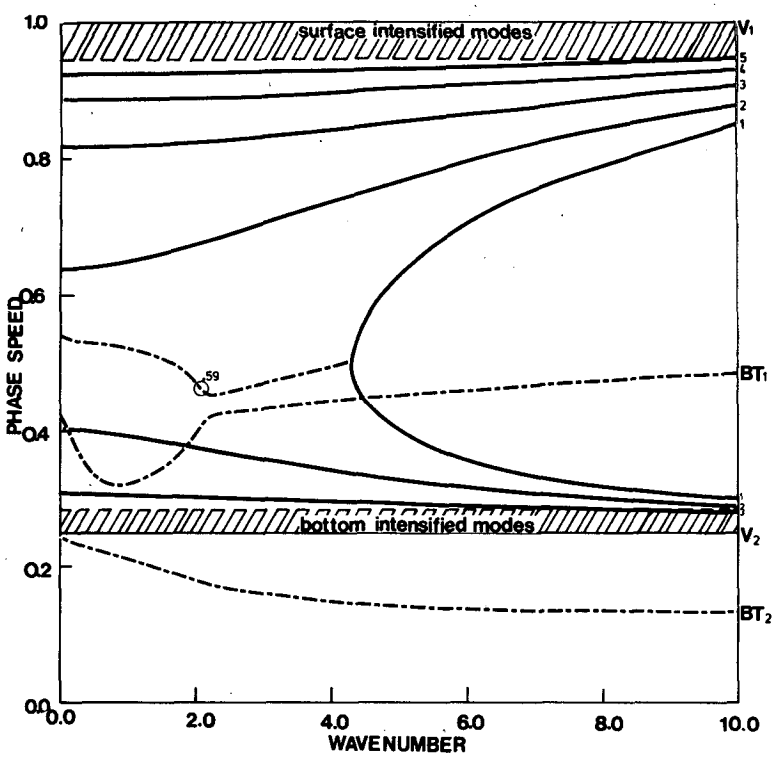

FIG. 14. As in Fig. 3 with $T = 0.0$ (no bottom slope).

are still the governing equations for the motion in the region $0 < x \leq 1$. In the region $1 < x \leq 1 + l_s$ the governing equation is that for barotropic flow above a sloping shelf.

$$(c - U_1)(\psi_{1xx} - k^2\psi_1) + (T_s + U_{1xx})\psi_1 = 0, \quad (4.1)$$

where $T_s = \alpha_s f L^2/Uh_1$. Eq. (4.1) may be combined with (2.2a) to give an upper layer equation,

$$(c - U)[(\psi_{1xx} - k^2\psi_1) + H(1 - x)F_1(\psi_2 - \psi_1)] + [H(1 - x)(U_2 - U_1)F_1 + U_{1xx} + H(x - 1)T_s]\psi_1 = 0, \quad (4.2)$$

where H is the Heaviside stepfunction [$H(\theta)$ is unity if θ is positive and is zero otherwise]. We wish to solve (4.2) and (2.2b) subject to the boundary conditions of no normal flow at solid boundaries,

$$\psi_n = 0, \quad n = 1, 2, \quad \text{at} \quad x = 0, \quad (4.3a)$$

$$\psi_1 = 0, \quad \text{at} \quad x = 1 + l_s, \quad (4.3b)$$

$$\psi_2 = 0, \quad \text{at} \quad x = 1. \quad (4.3c)$$

We consider a velocity profile of the form

$$U_1(x) = \begin{cases} V_1, & 0 < x \leq 1 \\ V_s, & 1 < x \leq 1 + l_s, \end{cases} \quad (4.4)$$

$$U_2(x) = V_2.$$

Such a profile gives a constant coefficient equation in the channel and shelf regions and the matching conditions at $x = 1$ on ψ_1 may be obtained as before. We find again that both $(c - U_1)\psi_{1x} + U_{1x}\psi_1$ and $\psi_1/(U_1 - c)$ must be continuous. The solution of (2.2), (4.2) for profile (4.4) subject to (4.3a, c) is

$$\left.\begin{aligned} \psi_1 &= b_1F_1 \sinh r_1x + b_2F_1 \sinh r_2x, \quad 0 \leq x < 1 \\ \psi_2 &= b_1R_1 \sinh r_1x + b_2R_2 \sinh r_2x, \quad 0 \leq x < 1 \end{aligned}\right\},$$

where b_1 and b_2 are arbitrary constants. The general solution of (4.2) for profile (4.4) subject to (4.3b) is

$$\psi_1 = b_3F_1 \sinh r_3(x - 1 - l_s) \quad 1 < x \leq 1 + l_s,$$

where b_3 is an arbitrary constant and $r_3^2 = T_s/(c - V_s) - k^2$. Applying the matching conditions at $x = 1$ gives the system

$$\mathbf{Bb} = \mathbf{0}, \quad (4.5)$$

where $b = (b_1, b_2, b_3)^T$ and

$$\mathbf{B} = \begin{pmatrix} R_1 \sinh r_1 & R_2 \sinh r_2 & 0 \\ (c - V_1)r_1 \cosh r_1 & (c - V_1)r_2 \cosh r_2 & (V_s - c)r_3 \cosh r_3 l_s \\ (c - V_s) \sinh r_1 & (c - V_s) \sinh r_2 & (c - V_1) \sinh r_3 l_s \end{pmatrix}.$$

The dispersion relation is given by requiring the determinant of **B** to vanish, i.e.,

$$R_1 \sinr_1[(c - V_1)^2 r_2 \cosr_2 \sinr_3 l_s + (c - V_s)^2 r_3 \cosr_3 l_s \sinr_2] - R_2 \sinr_2[(c - V_1)^2 r_1 \cosr_1 \sinr_3 l_s + (c - V_s)^2 r_3 \cosr_3 l_s \sinr_1] = 0. \quad (4.6)$$

For very short waves, $k \to \infty$, Eq. (4.6) becomes

$$\sinr_1 \sinr_2 \sinr_3 l_s = 0,$$

which has solutions $r_1 = m\pi$ or $r_2 = m\pi$ or $r_3 = m\pi/l_s, m = \pm 1, \pm 2, \pm 3, \ldots$. The first two solution sets are the channel modes of Mysak (1977) and the third set are topographic waves propagating along the shelf.

Fig. 16 gives a plot of the dispersion relation (4.6) for $l_s = 1$, $T_s = 12.5$, $V_s = 0$ and the other parameters as in Figs. 2 and 3. Once again, the curves for the baroclinic waves are similar to those of the channel flow for short longshore wavelength. There are now three regions with infinitely many discrete curves corresponding to high cross-stream wavenumber. The regions near $c = V_1$ and $c = V_2$ correspond to baroclinic channel waves and the region near $c = V_s$ corresponds to topographic shelf waves. Once again at the points I, II and III instabilities are present due to interaction between baroclinic waves of differing cross-stream structure. For longer waves the dispersion diagram deviates further from the channel case diagram than does the diagram for the open-ocean model. The additional set of topographic shelf waves causes more secondary instabilities. The growth rates of these instabilities are significantly larger than those of the secondary instabilities in the open-ocean model. There are now four mixed instabilities with growth rates of the same order as that of the gravest mode instability. There also are wave interactions which do not lead to instability. At the points IV, V and VI the first mode topographic shelf-wave interacts with lower layer concentrated baroclinic waves so that the dispersion curves do not cross. However, no instability is present.

Figs. 17–19 show the streamfunctions for the stable waves VII ($k = 3.44$, $c = 0.87$), VIII ($k = 2.41$, $c = 0.49$), and IV ($k = 4.6$, $c = 0.48$) of Fig. 16. Fig. 17 of wave VII shows an upper layer concentrated wave with antinode at the shelf boundary. The wave consists of a gravest mode shelf wave forcing a third-mode channel wave. Fig. 18 of wave VIII shows a wave comparable to the ocean-model wave VIII shown in Fig. 5. Once again, a gravest mode upper layer concentrated channel wave interacts with a third-mode lower layer wave. However, the interaction now forces a significant signal above the shelf. Fig. 19 of wave IV is included to show

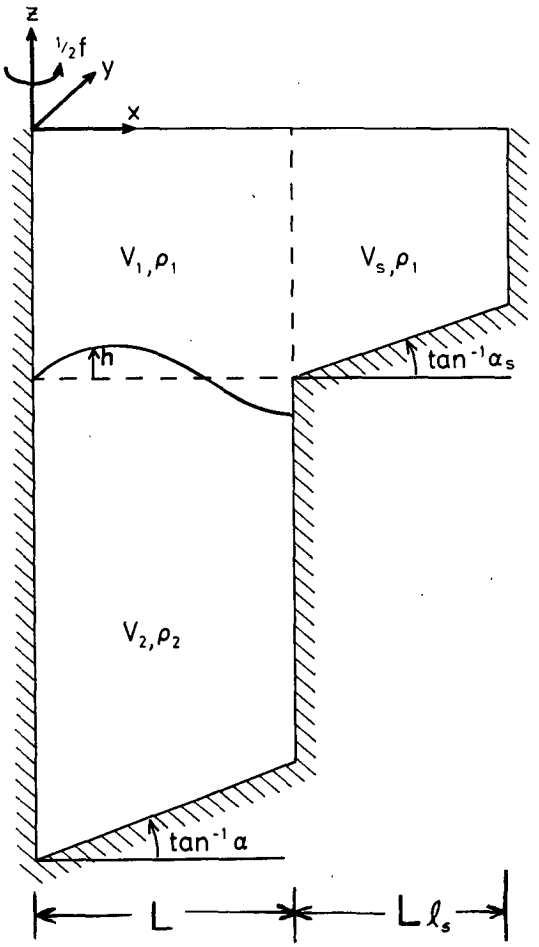

FIG. 15. Flow system considered in the shelf model. The nondimensional instantaneous interfacial weight due to the mean flow and traveling wave disturbance is given by $h = (V_2 - V_1)x + \phi_2 - \phi_1$.

that it is possible for a shelf wave to force significant motion in the deep channel layer. Here the lower layer response is far larger than that of the upper channel layer.

There is only one barotropic wave (BT in Fig. 16) caused by the horizontal shear in the upper layer. Table 2 includes the nondimensional growth of this wave which is unstable at all wavelengths. In the absence of vertical shear and topographic effects (i.e., $V_1 = V_2 = V$, $T = T_s = 0$), we have

$$F_1[(c - V)^2 \kappa \coth\kappa \tanh kl_s + k(c - V_s)^2] + F_2[(c - V)^2 k \coth k \tanh kl_s + k(c - V_s)^2] = 0. \quad (4.7)$$

The roots of (4.7) are a complex conjugate pair and so there will be one shear wave present which will be unstable at all wavelengths.

Fig. 20 gives the dispersion curves for the case of a stagnant lower channel layer and a weak current

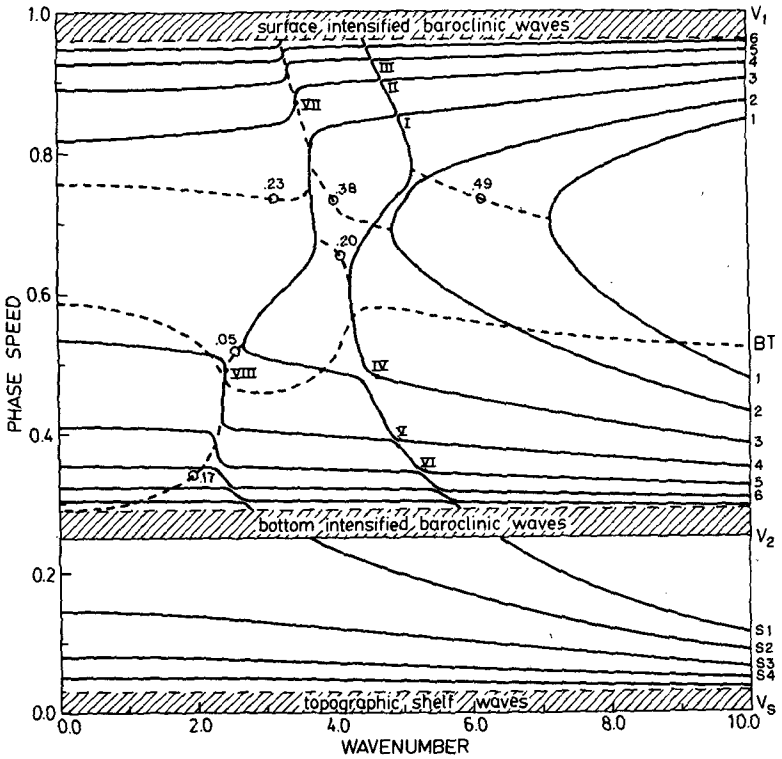

FIG. 16. Dispersion curves for the shelf model. The parameters V_1, V_2, F_1, F_2, and T are the same as in Fig. 2 and $T_s = 12.5$, $l_s = 1$, and $V_s = 0$. The shelf modes are numbered $S_1, S_2, \ldots$.

above the shelf region ($V_1 = 1, V_2 = 0, V_s = 0.25$). All other parameters are as in Fig. 16. The larger vertical shear in the channel causes higher growth rates in the channel mode instabilities (the gravest mode growth rate is increased by 40%). Once again, there are a large number of secondary instabilities, some with growth rates of the same order as the dominant instability. The weaker horizontal shear in the upper layer means that there is modification of

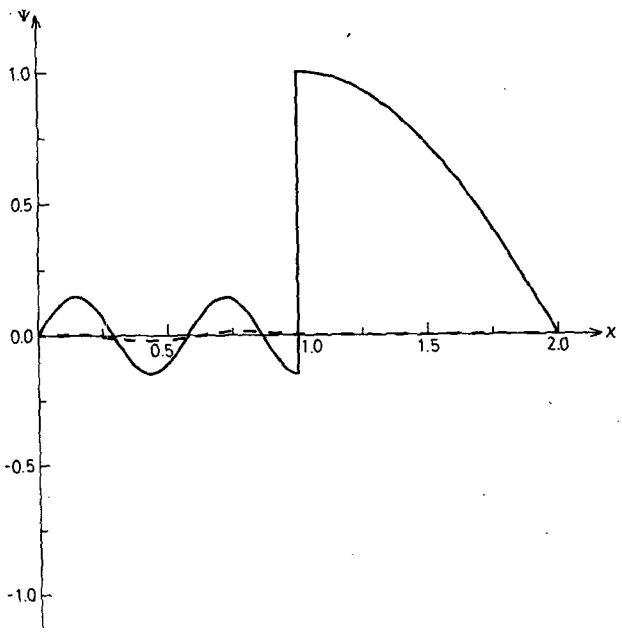

FIG. 17. Streamfunctions for the wave VII ($k = 3.44, c = 0.87$) of the shelf model. The coastal boundary is at $x = 2$ and the outer current boundary at $x = 0$.

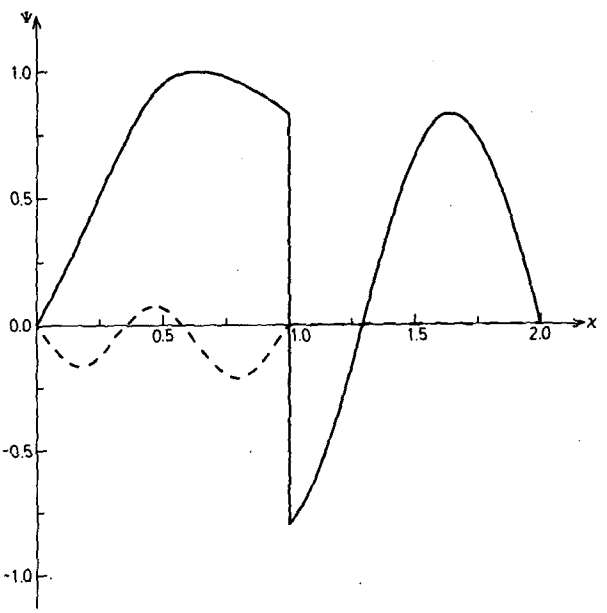

FIG. 18. Streamfunctions for the wave VIII ($k = 2.41, c = 0.43$) of the shelf model.

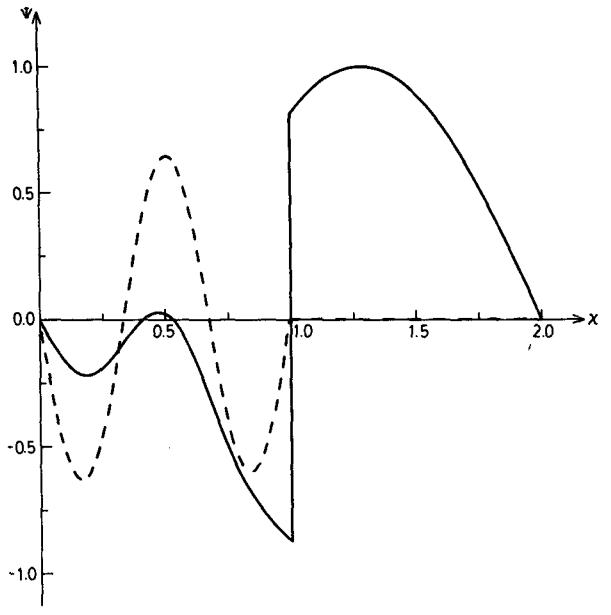

FIG. 19. Streamfunctions for the wave VI ($k = 4.6$, $c = 0.48$) of the shelf model.

the previously strong barotropic instability by baroclinicity and topography. The barotropic mode interacts with the upper layer concentrated waves and there are no long waves which may be ascribed directly to barotropic instability. Nondimensional growth rates for the unstable waves are given in Table 3.

TABLE 2. Nondimensional growth rates Im(kc) of the barotropically unstable wave in the shelf model with $F_1 = 27$, $F_2 = 6.8$, $T = 21$, $T_s = 12.5$, $l_s = 1$ and $V_s = 0$.

		Wavenumber k					
	V_1, V_2	1	2	4	6	8	10
FIG. 16	1, 0.25	0.11	0.23	0.76	2.31	3.50	4.59
FIG. 21	1, 0.1	0.07	0.23	0.67	2.19	3.42	4.54
FIG. 22	1, 0.0	—	—	0.50	2.11	3.37	4.50
FIG. 23	0.5, 0.0	0.01	0.04	0.31	0.73	1.52	2.14

5. Parameter study of shelf-model

We now discuss the effects of varying the shear, stratification and topographic parameters used in the previous section. In particular, because of the presence of three mean flow parameters (V_1, V_2 and V_s) in the shelf model, it is convenient to look at vertical shear and horizontal shear changes separately.

Figs. 21–23 show the dispersion curves for various values of the vertical shear $V_1 - V_2$, with $V_s = 0$ in each case. These figures represent variants of Fig. 16, where $V_s = 0$ also. As the vertical shear increases (see Figs. 16, 21 and 22), we note that the barotropically unstable wave (BT) interacts more and more with a second mode baroclinic wave and

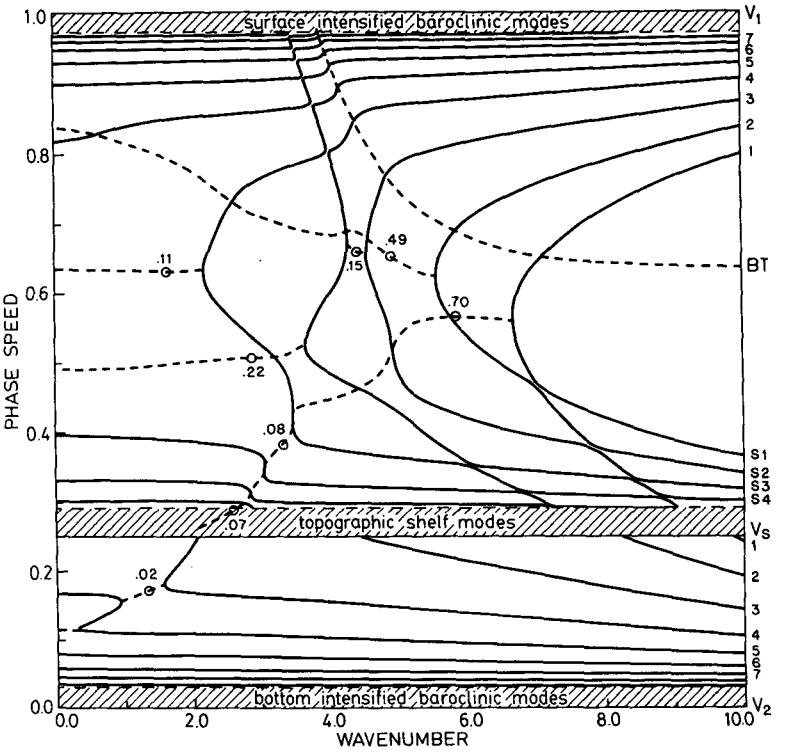

FIG. 20. Dispersion curves for the shelf model. The parameters are as in Fig. 8 with $V_2 = 0$, $V_s = 0.25$.

TABLE 3. Nondimensional growth rates Im(kc) of the barotropically unstable wave in the shelf model with $V_1 = 1, V_2 = 0.0$ and $l_s = 1$.

				Wavenumber k					
	V_s	F_1, F_2	T, T_s	1	2	4	6	8	10
FIG. 20	0.25	27, 6.8	21, 12.5	—	—	0.06	1.22	2.31	3.22
FIG. 24	0.5			—	—	—	0.38	1.16	1.90
FIG. 25	1.0			—	—	—	—	—	—
FIG. 26	0.25	54, 13.6	21, 12.5	—	—	0.02	1.03	1.87	2.85
FIG. 27	0.25	27, 6.8	0.0, 12.5	—	—	0.06	1.21	2.31	3.22
FIG. 28			21, 0.0	0.15	0.36	0.85	1.66	2.56	3.40
FIG. 29			0.0, 0.0	0.15	0.36	0.89	1.67	2.57	3.40

eventually becomes stable at low wavenumbers (see Fig. 22 and Table 2). However, while the BT wave is stabilized by increasing the vertical shear, the cross-channel mode instabilities and secondary instabilities tend to be destabilized. Decreasing the vertical shear (Fig. 23) produces rather weak cross-channel mode instabilities at generally higher frequencies and wavenumbers. The BT wave in this case also has reduced growth rates (see Table 2) and, at small wavenumbers, much lower phase speeds.

Figs. 24 and 25 show the effects of decreasing the horizontal shear in the upper layer and should be compared with Fig. 20. In all cases $V_1 = 1, V_2 = 0.0$ so that the vertical shear is kept constant. As $V_s \rightarrow V_1$, the growth rate and position [in (c, k) space] of the maximally unstable first-mode channel wave are not significantly changed. However, many new secondary instabilities arise which involve interactions between the topographic shelf modes S_n and the channel modes (see Fig. 24). Also, the BT wave gets pushed into the upper right corner in (c, k) space in this limit and has relatively small growth rates (see Table 3). When $V_s = V_1$ the BT wave, of course, disappears, but so do all the secondary instabilities. The resulting picture (Fig. 25) is relatively simple and, apart from the BT wave, is not unlike the case in Fig. 7, showing the open-ocean dispersion curves for $V_1 = 1.0, V_2 = 0.0$. However, the second-chan-

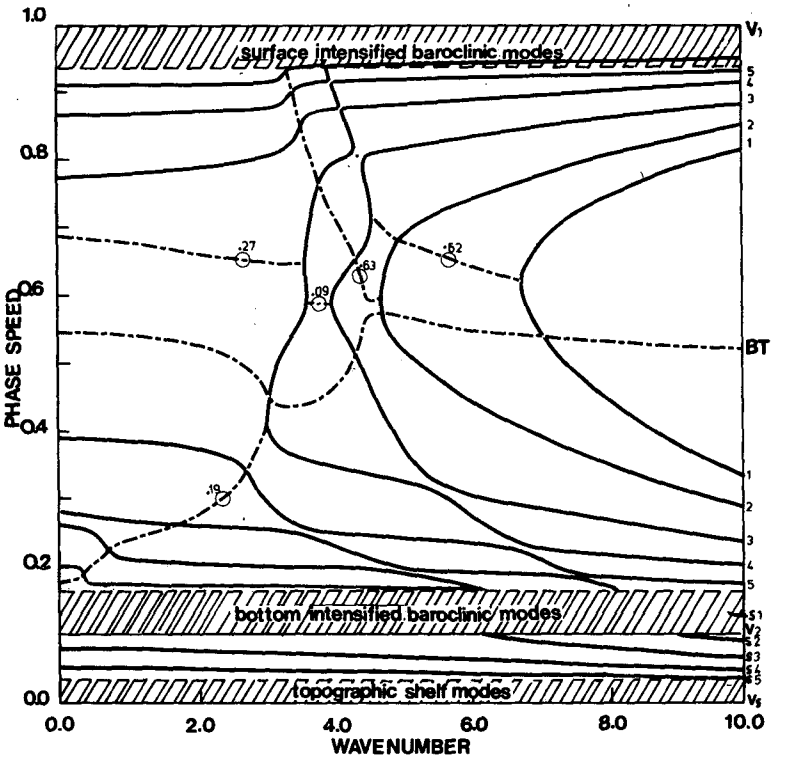

FIG. 21. As in Fig. 16 with $V_1 = 1, V_2 = 0.1$ (larger vertical shear).

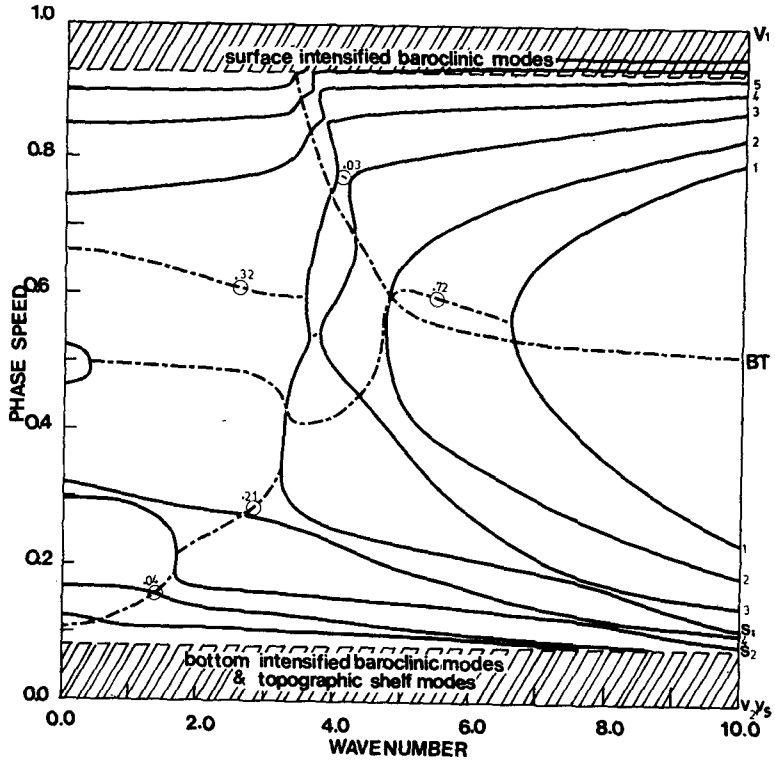

FIG. 22. As in Fig. 16 with $V_1 = 1$, $V_2 = 0.0$ (larger vertical shear).

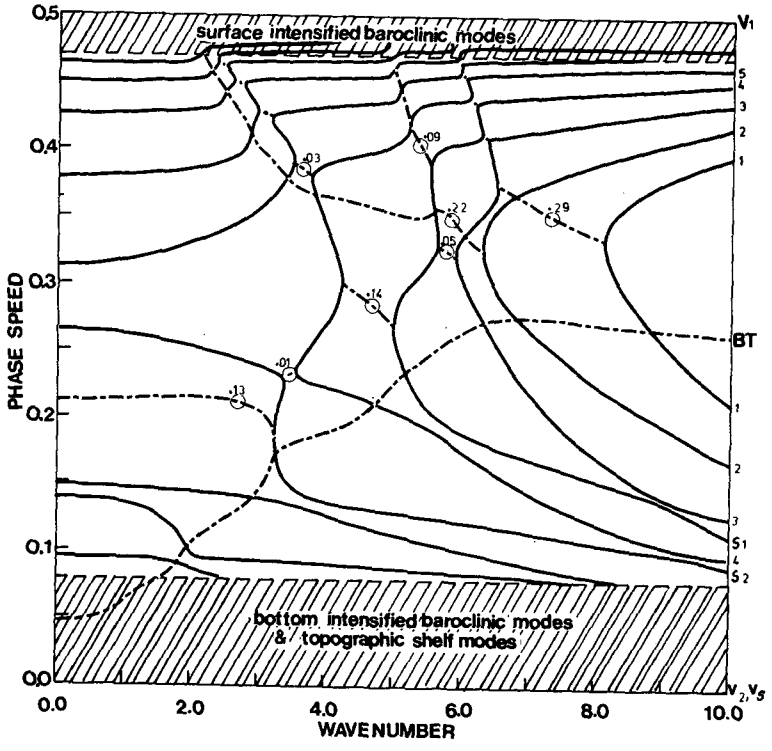

FIG. 23. As in Fig. 16 with $V_1 = 0.5$, $V_2 = 0.0$ (smaller vertical and horizontal shears).

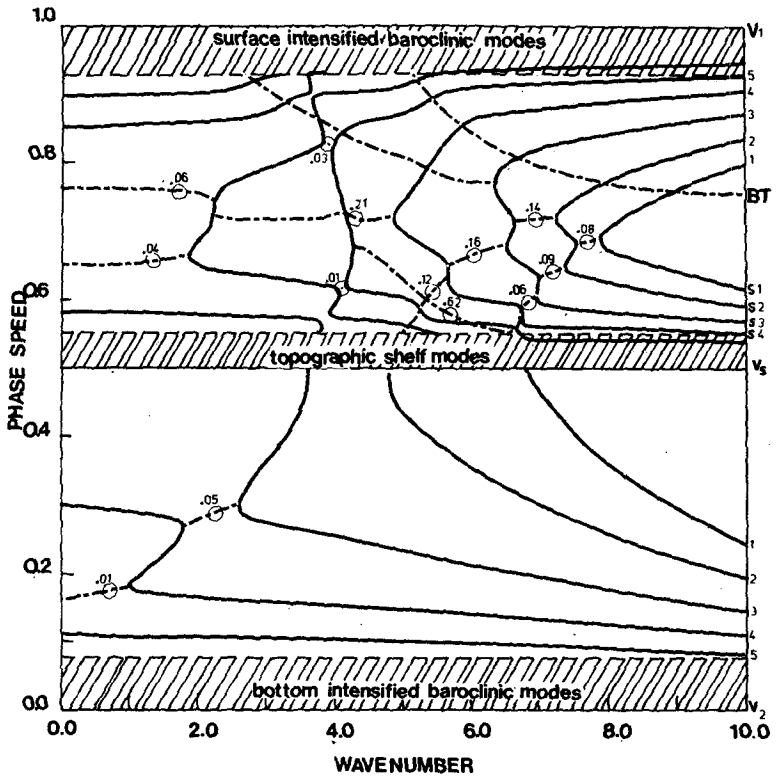

FIG. 24. As in Fig. 20, with $V_s = 0.5$ (smaller horizontal shear).

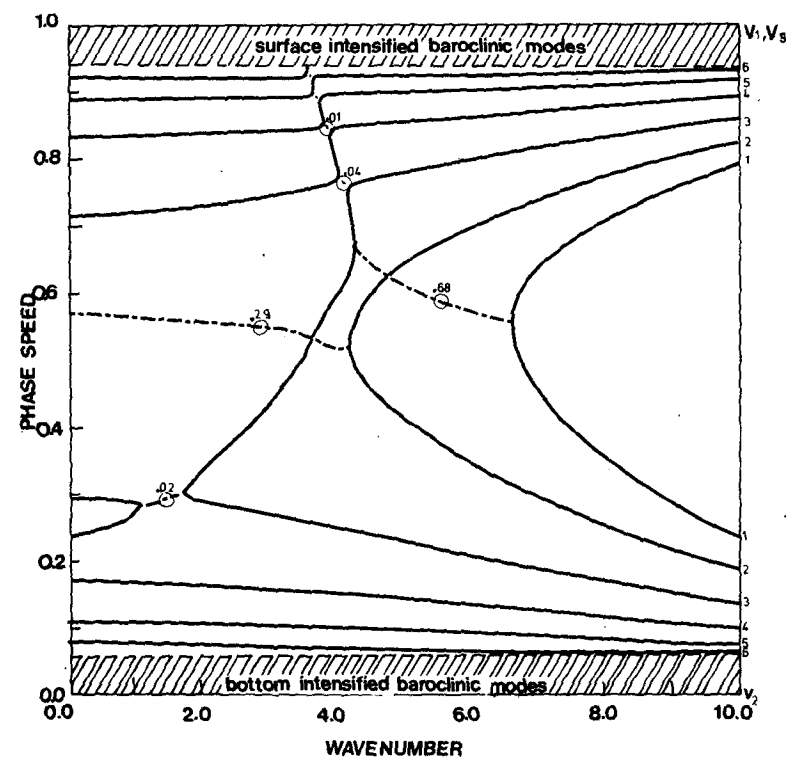

FIG. 25. As in Fig. 20 with $V_s = 1$ (no horizontal shear).

nel mode instability in Fig. 25 is unstable for all $k < 4.2$.

Fig. 26 shows the dispersion curves for a weaker stratification when $V_1 = 1.0$, $V_2 = 0.0$ and $V_s = 0.25$, as in Fig. 20. The growth rates of the first two-channel mode waves are substantially greater, and the wavenumber range of instability for these waves is much larger and includes much higher wavenumbers. The weaker stratification slightly stabilizes the BT wave (see Table 3), but otherwise leaves its position in (c, k) space unaltered.

Fig. 27 shows the effects of removing the bottom slope in the deep-channel region and should be compared with Fig. 20. It is interesting to note that the growth rates and wavenumber ranges of instability of the channel modes are considerably smaller in Fig. 27. Thus, in contrast to the open-ocean model where the continental rise exerts a stabilizing influence, here, in the presence of a neighboring sloping shelf, the continental rise has a strongly destabilizing influence on the baroclinically unstable waves. Fig. 28, on the other hand, shows the effects of replacing the sloping shelf by a flat shelf. Comparing Fig. 28 with Fig. 20, we note that the topographic shelf modes are now absent, and so are the secondary instabilities arising from the interactions between the shelf modes and the baroclinic channel modes. The growth rates of the primary instabilities are not much affected. The BT wave, funnily enough becomes destabilized when the shelf slope is removed (see Fig. 28 and Table 3). Finally, Fig. 29 shows the dispersion curves for a constant-depth shelf and channel. This limit ($T = 0.0 = T_s$) corresponds to a two-layer Eady model adjacent to a flat shelf. As might be anticipated the long baroclinic waves (modes 1 and 2) are unstable; but they have lower growth rates then when $T \neq 0$. The barotropic wave is virtually unaffected by the absence of bottom slope in the channel region (see last two lines in Table 3). Also, unlike in the case of the open-ocean Eady model (Fig. 14), there is no interaction between the BT wave and the baroclinically unstable waves.

6. Summary and discussion

Two variations have been made to the standard two-layer channel model for baroclinic instability. For the parameters used by Mysak (1977) to describe the California Undercurrent off Vancouver Island, the characteristics of the maximally unstable baroclinic wave in either the open-ocean or shelf model are within a few percent of those given by the channel model. It thus appears that the inclusion of vertical side walls at the edges of a coastal current flowing along the continental slope does not significantly affect the growth rate, frequency or wavelength of

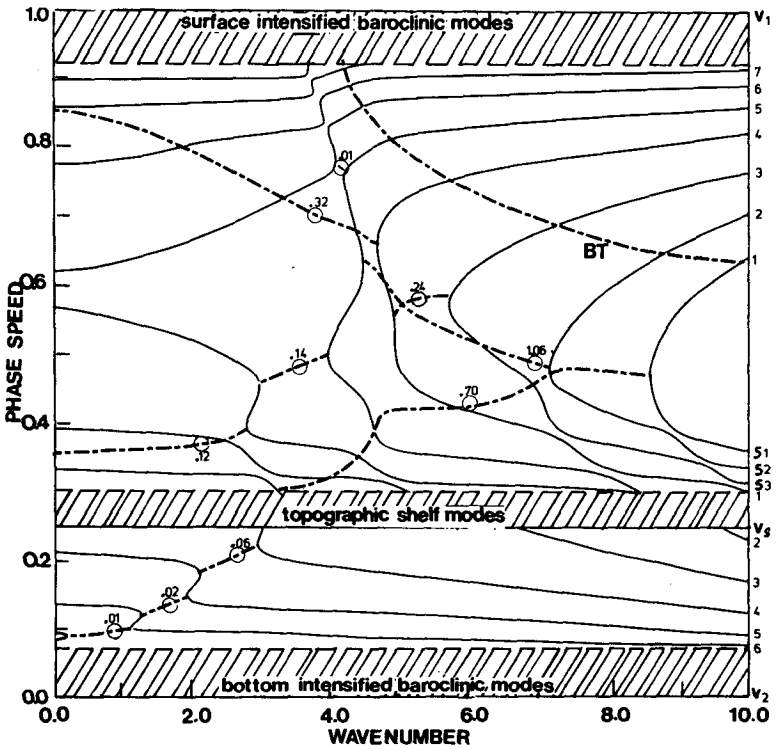

FIG. 26. As in Fig. 20 with $F_1 = 54$, $F_2 = 13.6$ (weaker stratification).

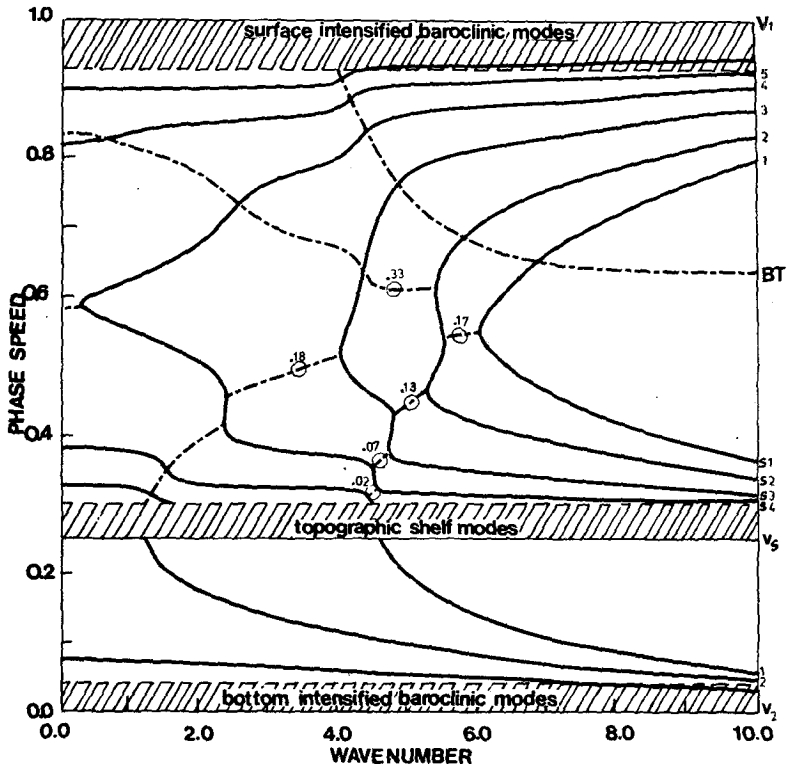

FIG. 27. As in Fig. 20 with $T = 0.0$ (no bottom slope in channel region).

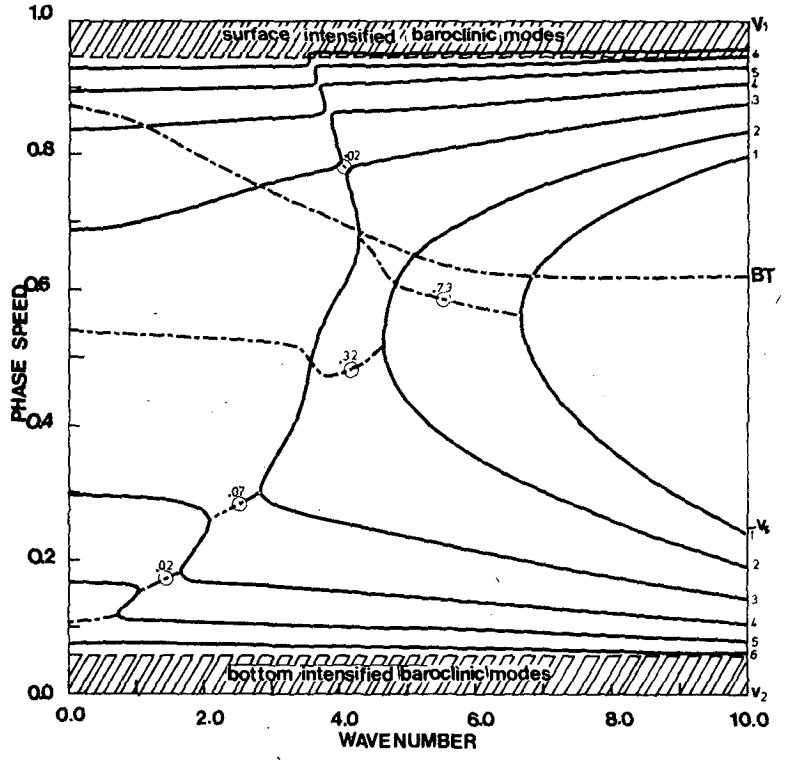

FIG. 28. As in Fig. 20 with $T_s = 0.0$ (no bottom slope in shelf region).

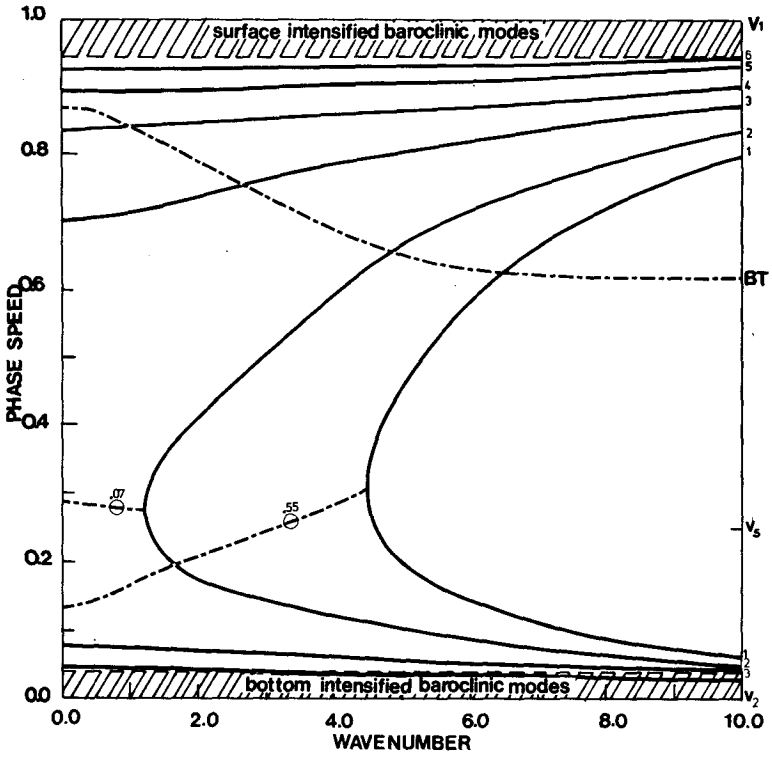

FIG. 29. As in Fig. 20 with $T = 0.0 = T_s$ (constant depth in both regions).

the maximally unstable wave, provided the wavelength is comparable to the channel width. Indeed, it is probably because of this theoretical result that surprisingly good agreement between observation and theory was obtained by Emery and Mysak (1980) who used the simple channel model to explain the presence of northward traveling thermal features in infrared satellite images off Vancouver Island.

In both the open ocean and shelf models secondary baroclinic instabilities at longer wavelengths are also possible and are the result of interactions between different cross-channel modes. However, their growth rates generally are small and thus the observations of such waves in nature would be unlikely.

Because of the concentrated horizontal shear in the mean flow (represented by a delta function), barotropic instabilities also were present in each model. The growth rates of these waves increased with wavenumber. However, at large wavenumbers such barotropically unstable disturbances would be confined to a very small region centered about the point of flow discontinuity. The observation of these waves in the ocean also would be unlikely because in practice coastal flows are not discontinuous in the horizontal direction. When the flow in each layer is modeled by a continuous velocity profile, no barotropic instabilities occur for parameters characteristic of the California Undercurrent (Wright, 1980).

From the parameter studies of the open-ocean and shelf models, it was found that the effect of varying the vertical shear, stratification or bottom slope was fairly predictable for the usual channel mode baroclinic instabilities. In general, the shear was destabilizing, whereas the stratification was stabilizing. In the open-ocean model, the continental rise was stabilizing, whereas in the shelf model (with a rigid outer wall and a sloping shelf), the continental rise was destabilizing. Topography also tends to increase the number of secondary interaction instabilities. In most cases, the barotropic instabilities were only moderately affected by changes in the vertical shear, stratification and bottom slope.

Finally we wish to point out two obvious limitations of the shelf model. First, in the shelf region the perturbation flow is assumed to be quasi-geostrophic. In reality, however, most low-frequency fluctuations on the shelf tend to be strongly aegeostrophic in the longshore direction (Allen, 1980). Thus to model accurately the coupling of the low-frequency offshore and shelf motions in the presence of coastal flows, a more general framework of the barotropic-baroclinic instability problem is required. Second, in order to avoid the frontal problem in the shelf model, we required that $V_2 - V_1 < 0$ (see Section 4). If $V_2 - V_1 \geq 0$, the interface could extend on to the shelf region, in which case water from the

deep continental slope region would rise up on to the shelf. To model this situation theoretically, a continuously stratified system would be required. Also, dissipative processes would not be negligible near where the interface rubs against the gently sloping shelf.

Acknowledgment. This work was supported by Operating and Strategic grants from the Natural Sciences and Engineering Research Council of Canada.

REFERENCES

Allen, J. S., 1980: Models of wind-driven currents on the continental shelf. *Annual Review of Fluid Mechanics*, Vol. 12, Annual Reviews, Inc., 389–433.

Cutchin, D. L., and D. B. Rao, 1976: Baroclinic and barotropic edge waves on a continental shelf. Spec. Rep. No. 30, Center for Great Lake Studies, University of Wisconsin, Milwaukee, 53 pp.

Drazin, P. G., and L. N. Howard, 1966: Hydrodynamic stability of parallel flow of inviscid fluid. *Advances in Applied Mechanics*, Vol. 9, Academic Press, 1–89.

Emery, W. J., and L. A. Mysak, 1980: Dynamical interpretation of satellite sensed thermal features off Vancouver Island. *J. Phys. Oceanogr.*, **10**, 961–970.

Gent, P. R., 1975: Baroclinic instability of slowly varying zonal flow. Part 2. *J. Atmos. Sci.*, **32**, 2094–2102.

Gill, A. E., and A. J. Clarke, 1974: Wind-induced upwelling, coastal currents and sea-level changes. *Deep-Sea Res.*, **21**, 325–345.

Hart, J. E., 1974: On the mixed stability problem for quasi-geostrophic ocean currents. *J. Phys. Oceanogr.*, **4**, 349–356.

Helbig, J. A., 1978: On the inertial stability of coastal flows. Ph.D. thesis, University of British Columbia, Vancouver, 183 pp.

Killworth, P. D., 1980: Barotropic and baroclinic instability in rotating stratified fluids, with application to geophysical fluid systems. *Dyn. Atmos. Oceans*, **4**, 143–184.

Kubota, M., 1977: Long-period topographic trapped waves in a two-layer ocean with basic flow. *J. Oceanogr. Soc. Japan*, **33**, 199–206.

McIntyre, M. E., 1970: On the non-separable baroclinic parallel flow instability problem. *J. Fluid Mech.*, **40**, 273–306.

Mysak, L. A., 1977: On the stability of the California Undercurrent off Vancouver Island. *J. Phys. Oceanogr.*, **7**, 904–917.

——, 1980: Recent advances in shelf wave dynamics. *Rev. Geophys. Space Phys.*, **18**, 211–241.

——, and F. Schott, 1977: Evidence for baroclinic instability of the Norwegian current. *J. Geophys. Res.*, **82**, 2087–2095.

Orlanski, I., and M. D. Cox, 1973: Baroclinic instability in ocean currents. *Geophys. Fluid Dyn.*, **4**, 297–332.

Pedlosky, J., 1964: The stability of currents in the atmosphere and the ocean: Part 1. *J. Atmos. Sci.*, **21**, 201–219.

——, 1979: *Geophysical Fluid Dynamics*. Springer-Verlag, 624 pp.

Smith, P. C., 1976: Baroclinic instability in the Denmark Strait overflow. *J. Phys. Oceanogr.*, **6**, 335–371.

Stone, P. H., 1969: The meridional structure of baroclinic waves. *J. Atmos. Sci.*, **26**, 376–389.

Wright, D. G., 1980: On the stability of a fluid with a specialized density stratification. Part II: Mixed baroclinic-barotropic instability with application to the northeast Pacific. *J. Phys. Oceanogr.*, **10**, 1307–1322.